Beer-Lambert law in the time domain

M. Žitnik,[1] Š. Krušič,[2] K. Bučar,[1] and A. Mihelič[1]
[1]*J. Stefan Institute, Jamova Cesta 39, 1000 Ljubljana, Slovenia*
[2]*Faculty of Mathematics and Physics, University of Ljubljana, Jadranska 19, 1000 Ljubljana, Slovenia*

(Received 29 March 2018; published 29 June 2018)

According to the Beer-Lambert law, the spectral density of weak electromagnetic radiation is attenuated exponentially, with the characteristic length depending on atomic density and the frequency-dependent photoabsorption cross section of the target. We discuss an analog of the Beer-Lambert law in the time domain, showing that the temporal profile of the initial light pulse enters explicitly into each term of expansion of the exponential function as a multiconvolution with the corresponding temporal response of an atom. The form invokes a description of pulse propagation in terms of the temporal base functions, which may be precalculated for a chosen initial pulse shape, allowing us to obtain the attenuated profile at a given target depth simply by summing up a sufficient number of weighted base functions. The variant with a 100-fs initial Gaussian pulse is worked out in detail, with the atomic response exhibiting either pure exponential or mixed prompt-exponential decay, characteristic of a photoexcited bound state or a Fano resonance. The method is shown to be valid for an arbitrary temporal profile of the initial electric field and is illustrated for pulses resonantly tuned to the low-lying doubly excited states of the He atom.

DOI: 10.1103/PhysRevA.97.063424

I. INTRODUCTION

Experiments with synchrotron light are an important tool to unravel the structure and relaxation dynamics of various materials. In this regard, photoabsorption is one of the most common and useful techniques [1]. It relies on the Beer-Lambert(-Bouguer) (BL) law [2–4] which, in modern language, relates the photoabsorption cross section $\sigma(\omega)$ to attenuation of light with the frequency component ω. Denoting the target thickness by z and the atomic target density by N, the spectral density at the target exit is given by

$$I(z,\omega) = I(0,\omega)e^{-\sigma(\omega)Nz}, \tag{1}$$

where $I(0,\omega)$ is spectral density of light at the target entrance. The exponential law stems from a very general assumption, according to which the reduction of light intensity in target thickness dz is proportional to the light intensity of the same color that hits the target layer. Suppose that the incident light has a Gaussian spectrum $I_{\omega_0}(0,\omega)$, centered at ω_0. If there are no atomic resonances in the vicinity of ω_0 and the spectral width of the incident light is reasonably small, $\sigma(\omega) \approx \sigma(\omega_0)$ and spectral density $I_{\omega_0}(0,\omega)e^{-\sigma(\omega_0)Nz}$ at the target exit is an attenuated replica of the entrance spectrum. This is a typical situation encountered at synchrotron light sources when the photon energy is set above the lowest threshold and away from any higher ionization threshold of the target.

Next we consider the Gaussian light pulse to be resonant with a single isolated bound state at energy ω_i above the target ground state. According to (1), the spectrum of the transmitted pulse is

$$I(z,\omega) = I_{\omega_i}(0,\omega)e^{-\sigma_i(\omega)Nz}, \tag{2}$$

where $\sigma_i(\omega) = (\sigma_i\Gamma_i/2\pi)/[(\omega-\omega_i)^2+\Gamma_i^2/4]$ is a product of the energy-integrated photoabsorption cross section $\sigma_i = 4\pi^2\alpha\omega_i|d_{0i}|^2$ [5] and a (normalized) Lorentzian [6], $d_{0i} = d_{i0}^*$ is a length-form dipole matrix element for the transition from the ground (0) to the excited state (i) of the target atom, and Γ_i is the total probability decay rate of the excited state. Equation (2) obviously implies a change of the entrance spectrum: If the target thickness and/or target density are large enough, the spectrum of the transmitted light acquires a "hole in the center" due to enhanced photoabsorption at resonance energy ω_i. The total intensity of light at target depth z is

$$I(z) = \int_0^\infty I(z,\omega)d\omega. \tag{3}$$

Obviously, the BL law applies for weak light only. In the present context, weak light is to be understood as light whose intensity is low enough so that $|Fd_{0i}t_0| \ll 1$, where t_0 denotes the pulse duration, Fd_{0i} is the Rabi frequency of the $0 \leftrightarrow i$ transition, and F is the magnitude of the electric field making up the pulse ($I \propto |F|^2$) [7].

Apart from its spectrum, the temporal profile of the transmitted pulse is a measurable quantity too. Photoabsorption studies in the time domain offer complementary insight because the light pulse is not completely defined by its spectrum. While the Fourier transform $\mathcal{F}[F(\omega)](t)$, acting on the *field*, translates between the temporal and spectral representations of the problem [$F(\omega) \leftrightarrow F(t)$], according to the Wiener-Khinchin theorem [8], the Fourier transform of the spectrum proportional to $|F(\omega)|^2$ is proportional only to the field autocorrelation function $\gamma(\Delta)$, defined by

$$\int_{-\infty}^{\infty} F(t)F^*(t+\Delta)dt \propto \mathcal{F}[|F(\omega)|^2](\Delta). \tag{4}$$

The information missing in the spectrum is knowledge about the relative phases of the electric field for each frequency

component of the pulse which may affect the outcome of the absorption process. In fact, light pulses with equal spectra but different degrees of coherence (different extent of phase alignment) result in the same field autocorrelation function (4) but have different temporal intensity profiles (and vice versa). While $\gamma(\Delta)$ can be readily measured by a Michelson interferometer and is just another type of spectroscopy [9], a direct measurement of the intensity in the time domain requires a temporal resolution better than the pulse duration. Soon after the discovery of the laser, the capability to produce short pulses surpassed the ability to directly measure their duration and until today the situation has not changed. Still, from its invention [10], streak camera technology has advanced from the initial nanosecond regime to the recently achieved 100-fs resolution [11], steadily improving the possibility of performing direct temporal imaging of short light pulses in different wavelength regions.

Below we discuss an analog of Eq. (1) in the time domain. We start by solving the Maxwell-Bloch equations for the case of near-resonant weak-light propagation in an atomic medium. The solution is written in the form of a series and is shown to apply for an arbitrary initial temporal dependence of the electric field by comparison with a direct numerical solution of the field propagation equation. A case with a coherent incident Gaussian pulse is worked out in detail and the corresponding solution for electric field is converted to the spectral domain to show that it fully complies with the BL law. The phenomenon of free-induction decay (FID) [12,13], leading to delayed fluorescence, is shown to depend crucially on the degree of coherence for pulses with the same temporal intensity profile. Finally, the same framework is employed to study propagation of weak pulses tuned to a Fano resonance [14]. The corresponding time-dependent solution is shown to result in the same attenuation of total pulse intensity as a direct application of BL law with the well-known Fano photoabsorption profile. The results are illustrated by calculating attenuation of 100-fs-long pulses with photon frequency tuned to the selected He doubly excited states featuring lifetimes on different scales with respect to the initial pulse duration.

II. SINGLE BOUND STATE

A. Time domain

We examine attenuation of a resonant light pulse in the time domain, assuming incident intensity to be so low that the majority of atoms along the incident beam remain in the initial ground state. However, the light itself may be absorbed strongly while passing a given length z in the target. The pulse is set to travel along the positive z direction and we may think of it as starting up as a Gaussian

$$I(z,t) \propto |F(z,t)|^2 \propto e^{-[t-(z+Z_0)/c]^2/2t_0^2}, \tag{5}$$

which at time $t = 0$ is centered at $z = -Z_0$, i.e., outside the target. In the weak-light approximation, the evolution of the electric field in the target is governed by two coupled Maxwell-Bloch (MB) equations that relate the field amplitude $F(z,t)$ to the coherence ρ_{0i} between the lower and upper atomic states:

$$\frac{1}{c}\frac{\partial F}{\partial t} + \frac{\partial F}{\partial z} = \frac{2\pi i \omega_i d_{i0} N}{c}\rho_{0i}, \tag{6}$$

$$\dot{\rho}_{0i} = -\frac{\Gamma_i}{2}\rho_{0i} + i d_{0i} F. \tag{7}$$

The above form follows from the MB equations describing a two-level system (see Ref. [7], p. 185) by taking into account that the ground-state and excited-state populations $\rho_{00} \approx 1$ and $\rho_{ii} \ll 1$, respectively, at all times. The excited state is considered to be a single bound state with a finite lifetime Γ_i^{-1}. The speed of light is defined as $c = 1/\alpha$, where α is the fine-structure constant. Atomic units are used throughout the paper.

We proceed by formally solving Eq. (7),

$$\rho_{0i}(z,t) = i d_{0i} \int_0^t F(z,t') e^{-\Gamma_i (t-t')/2} dt', \tag{8}$$

where we have taken into account that $\rho_{0i}(z,0) = 0$. The coherence at a given location builds up due to the presence of the field prior to the time t which is "forgotten" exponentially with characteristic time $(\Gamma_i/2)^{-1}$. Inserting the solution (8) into Eq. (6) and removing the time retardation by switching to the local time $\tau = t - z/c - Z_0/c$, the field amplitude obeys the equation

$$\frac{\partial F(z,\tau)}{\partial z} = -\frac{\beta_i}{2}\int_{-\infty}^{\tau} F(z,\tau') e^{-\Gamma_i(\tau-\tau')/2} d\tau'. \tag{9}$$

Evolution of the amplitude is thus determined by its initial temporal profile $F(0,\tau)$, by decay rate Γ_i, and by the parameter $\beta_i = 4\pi\alpha\omega_i |d_{0i}|^2 N$. The solution of the above partial integro-differential equation may be constructed by following a general iterative variational scheme,

$$F^{(n+1)}(z,\tau) = F^{(n)}(z,\tau) - \int_0^z \left[\frac{\partial F^{(n)}(\xi,\tau)}{\partial \xi} + \frac{\beta_i}{2}\int_{-\infty}^{\tau} F^{(n)}(z,\tau') e^{-\Gamma_i(\tau-\tau')/2} d\tau'\right] d\xi,$$

discussed by Hussain *et al.* [15]. One starts with the initial pulse shape $F^{(0)} = F_0(\tau)$ to generate

$$F^{(1)}(z,\tau) = F_0(\tau) - \frac{\beta_i z}{2}\int_{-\infty}^{\tau} F_0(\tau') e^{-\Gamma_i(\tau-\tau')/2} d\tau'.$$

The second iteration gives

$$\begin{aligned} F^{(2)}(z,\tau) &= F^{(1)}(z,\tau) - \int_0^z \left[\frac{\partial F^{(1)}(\xi,\tau)}{\partial \xi} + \frac{\beta_i}{2}\int_{-\infty}^{\tau} F^{(1)}(z,\tau') e^{-\Gamma_i(\tau-\tau')/2} d\tau'\right] d\xi \\ &= F_0(\tau) - \frac{\beta_i z}{2}\int_{-\infty}^{\tau} F_0(\tau') e^{-\Gamma_i(\tau-\tau')/2} d\tau' - \int_0^z \left[-\frac{\beta_i}{2}\int_{-\infty}^{\tau} F_0(\tau') e^{-\Gamma_i(\tau-\tau')/2} d\tau'\right. \end{aligned}$$

$$+\frac{\beta_i}{2}\int_{-\infty}^{\tau}\left\{F_0(\tau')-\frac{\beta_i z}{2}\int_{-\infty}^{\tau'}F_0(\tau'')e^{-\Gamma_i(\tau'-\tau'')/2}d\tau''\right\}e^{-\Gamma_i(\tau-\tau')/2}d\tau'\Big]d\xi$$
$$=F_0(\tau)-\frac{\beta_i z}{2}\int_{-\infty}^{\tau}F_0(\tau')e^{-\Gamma_i(\tau-\tau')/2}d\tau'+\frac{\beta_i^2 z^2}{8}\int_{-\infty}^{\tau}e^{-\Gamma_i(\tau-\tau')/2}\int_{-\infty}^{\tau'}F_0(\tau'')e^{-\Gamma_i(\tau'-\tau'')/2}d\tau''d\tau'.$$

One can readily show that the solution of Eq. (9) is given by the series expansion

$$F(z,\tau)=F_0(\tau)-\frac{\beta_i z}{\Gamma_i}[E*F_0](\tau)+\frac{\beta_i^2 z^2}{2\Gamma_i^2}[E*E*F_0](\tau)+\cdots$$
$$=\sum_{n=0}^{\infty}(-1)^n\frac{\beta_i^n z^n}{n!\Gamma_i^n}F_n(\tau), \tag{10}$$

where $F_n(\tau)$ denotes the n-fold convolution of the initial pulse with the exponential decay function $E(\tau)=(\Gamma_i/2)e^{-\Gamma_i\tau/2}$. The temporal profile of the field amplitude at the target exit is thus given by the expansion of $e^{-\beta_i z F_0(\tau)/\Gamma_i}$, where the nth term is proportional to the n-fold convolution $F_n(\tau)$ of the initial pulse field $F_0(\tau)$ and not to the field $F_0(\tau)$ to the nth power. When $\beta_i z/\Gamma_i \ll 1$, i.e., whenever the dipole coupling, target length, target density, and/or resonance lifetime are small, a few terms of (10), if not one, may be enough to calculate the pulse shape at a given target depth from the known temporal profile of the initial pulse. Pulse attenuation is always associated with a change of its temporal profile. Namely, in the $\Gamma_i\to\infty$ limit, $F_n\to F_0$ for all n and consequently $F(z,\tau)=F_0(\tau)e^{-\sigma_i(\omega_i)Nz/2}$. However, such an instant decay limit corresponds to the absorption by an "infinitely broad" bound state and leads to zero attenuation, the same as absorption of a flat, nonresonant photoabsorption continuum with the vanishing cross section $\sigma_i(\omega_i)=2\sigma_i/\pi\Gamma_i=2\beta_i/N\Gamma_i$.

In the expression (10), the spatial and temporal dependence are clearly separated in each term of the series. Let us refer to F_n as temporal base field profiles. These profiles are characteristic of a given initial pulse profile and resonance type. When known, they enable a straightforward calculation of the exit pulse for any target depth. In fact, to construct F_n for given n, only a single convolution with the initial pulse is required. To see this, first the n-fold self-convolution of the exponential function is performed by applying the convolution theorem for Fourier transform $\mathcal{F}$, namely,

$$E*E*\cdots*E=\mathcal{F}^{-1}[\mathcal{F}[E]\mathcal{F}[E]\cdots\mathcal{F}[E]]. \tag{11}$$

The right-hand side of (11) can be easily calculated and the desired expression is obtained by a single convolution of the above result with the initial pulse,

$$F_n(\tau)=\frac{(\Gamma_i/2)^n}{(n-1)!}\int_{-\infty}^{\tau}(\tau-\tau')^{n-1}e^{-\Gamma_i(\tau-\tau')/2}F_0(\tau')d\tau'. \tag{12}$$

When the initial pulse intensity follows a Gaussian (5), the corresponding amplitude of the coherent field is $F_0(\tau)=(2t_0\sqrt{\pi})^{-1}e^{-\tau^2/4t_0^2}$. By introducing a new variable $x=(\tau-\tau')/2t_0$, Eq. (12) becomes

$$F_n^G(\tau)=\frac{\Gamma_i^n t_0^{n-1}}{2\sqrt{\pi}(n-1)!}e^{-\tau^2/4t_0^2}\times\int_0^{\infty}x^{n-1}e^{-x^2-x(\Gamma_i t_0-\tau/t_0)}dx. \tag{13}$$

The solution of the above integral is known (see Ref. [16], Sec. 3.462):

$$F_n^G(\tau)=\frac{\Gamma_i^n t_0^{n-1}F_0(\tau)}{2(n-1)!}\Bigg[t_0\Gamma_i\left(\frac{n}{2}\right){}_1F_1\left(\frac{n}{2},\frac{1}{2};\frac{(\tau-\Gamma_i t_0^2)^2}{4t_0^2}\right)$$
$$+(\tau-\Gamma_i t_0^2)\Gamma_i\left(\frac{n+1}{2}\right)$$
$$\times{}_1F_1\left(\frac{n+1}{2},\frac{3}{2};\frac{(\tau-\Gamma_i t_0^2)^2}{4t_0^2}\right)\Bigg]. \tag{14}$$

The confluent hypergeometric function has been denoted by ${}_1F_1(a,b;x)$ [17].

Explicit expressions for $1\leqslant n\leqslant 4$ are given by

$$F_1^G=\frac{\Gamma_i t_0}{2}e^{T^2}\sqrt{\pi}[1+\mathrm{erf}(T)]F_0(\tau),$$
$$F_2^G=\frac{(\Gamma_i t_0)^2}{2}\left\{1+e^{T^2}\sqrt{\pi}T[1+\mathrm{erf}(T)]\right\}F_0(\tau),$$
$$F_3^G=\frac{(\Gamma_i t_0)^3}{8}\left\{2T+e^{T^2}\sqrt{\pi}(1+2T^2)[1+\mathrm{erf}(T)]\right\}F_0(\tau),$$
$$F_4^G=\frac{(\Gamma_i t_0)^4}{24}\Big\{2(1+T^2)$$
$$+e^{T^2}\sqrt{\pi}T(3+2T^2)[1+\mathrm{erf}(T)]\Big\}F_0(\tau). \tag{15}$$

For convenience, the variable $T=(\tau-\Gamma_i t_0^2)/2t_0$ has been introduced above. As an example, the base temporal field profiles for a Gaussian initial pulse are presented in Fig. 1 for three fictitious bound states, denoted by na^*, because their resonant energies and decay widths were chosen to match those of the corresponding $na\,{}^1P_1$ doubly excited states below the $N=2$ ionization threshold of He. At the chosen target conditions, the attenuated pulse shows damped field oscillations for the fastest decaying $2a^*$ state. This is emphasized for the $3a^*$ state that has the lifetime comparable to the initial pulse duration. For the long-lived $7a^*$ state the outgoing field acquires a long tail and an extra phase difference π that decays with the characteristic time $2/\Gamma_i$. These temporal profiles bear clear signatures of

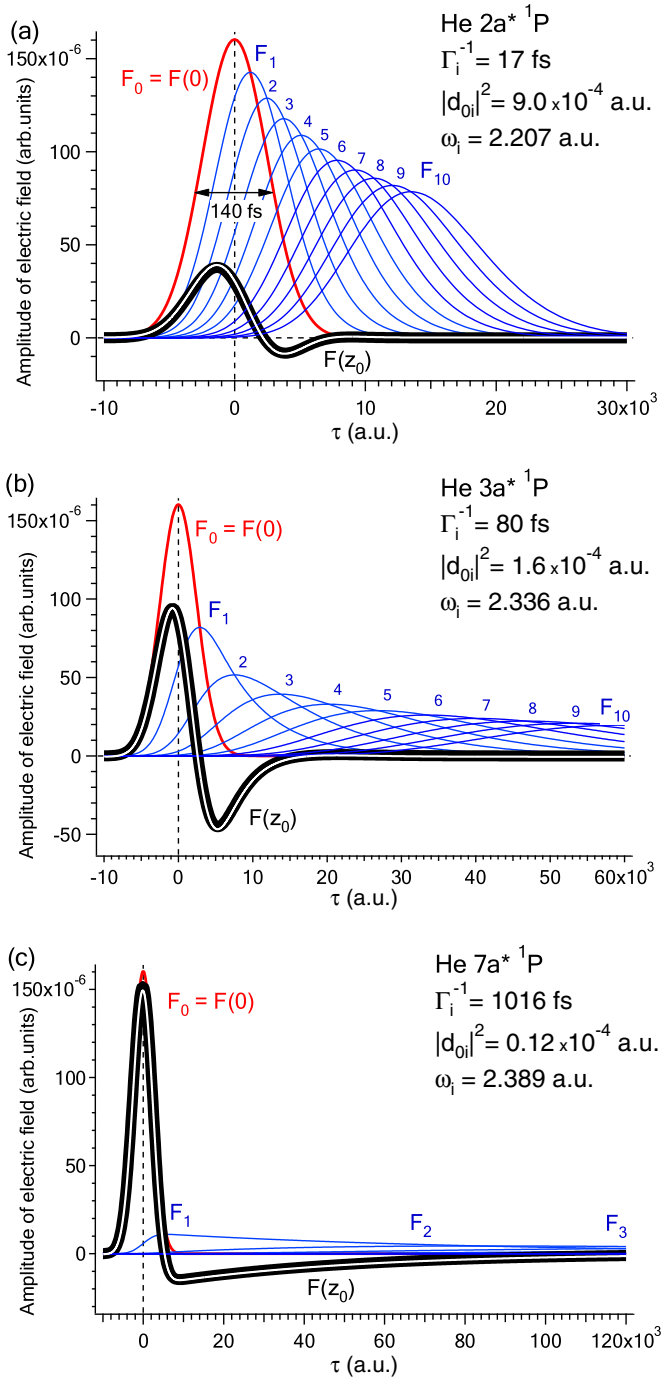

FIG. 1. Initial $100\sqrt{2}$-fs FWHM Gaussian pulse of electric field amplitude $F_0(\tau)$ (red curve) together with temporal base field functions $F_n(\tau)$ (blue curves) for $1 \leqslant n \leqslant 10$. At given target depth z the pulse is obtained by a linear combination of the temporal base field functions weighted by $(\beta_i z/\Gamma_i)^n/n!$. Black thick curves show the attenuated electric field amplitude after passing the $z_0 = 2$ cm distance in He gas at 1000 Pa. The initial pulse is tuned to (a) the $2a^*$ state ($\beta_i z_0/\Gamma_i = 1.84$), (b) the $3a^*$ state ($\beta_i z_0/\Gamma_i = 1.56$), and (c) the $7a^*$ state ($\beta_i z_0/\Gamma_i = 1.51$). The white curve shows the numerical solution of the full two-level MB equations not constrained by the weak-light approximation. Excitation energies ω_i and decay widths Γ_i of bound states are taken from [18].

a free-induction decay where the energy, accumulated in the atomic coherence ρ_{0i}, is either released steadily after the main pulse has gone [Fig. 1(c)] or exchanged several times with the main pulse if the lifetime of the bound state is shorter than the pulse duration [Figs. 1(a) and 1(b)].

Turning back to the general case (10), we note that the convolution with an area normalized function preserves the integral of the original pulse. This implies that

$$\int_{-\infty}^{\infty} F(z,\tau)d\tau = e^{-\beta_i z/\Gamma_i}\int_{-\infty}^{\infty} F_0(\tau)d\tau, \tag{16}$$

i.e., the integral over time of the *field amplitude* decays exponentially with z. The above equation holds for an arbitrary temporal profile of the initial pulse until the light intensity is weak.

The BL law, however, deals with attenuation of light intensity. The integral of the modulus square of the electric field amplitude over time is proportional to the total number of photons passing a given target position in the corresponding time interval. Using Eq. (10), the required integral is expressed by

$$\int_{-\infty}^{\infty} |F(z,\tau)|^2 d\tau = \left(\int_{-\infty}^{\infty} |F_0(\tau)|^2 d\tau\right)\sum_{p=0}^{\infty}\frac{(-2\beta_i z)^p g_p}{\Gamma_i^p\, p!}. \tag{17}$$

Each term in the expansion is weighted by an absorption factor $g_p = \int_{-\infty}^{\infty} G_p(\tau)d\tau / \int_{-\infty}^{\infty} |F_0(\tau)|^2 d\tau$, where the corresponding temporal base intensity function

$$G_p(\tau) = 2^{-p}\sum_{q=0}^{p}\binom{p}{q} F_q(\tau)F_{p-q}^*(\tau) \tag{18}$$

depends on multiple temporal base field functions (12). Obviously, $g_0 = 1$ for any pulse shape, and keeping only this term in Eq. (17) corresponds to pulse propagation without any absorption. The first nontrivial absorption factor is given by

$$g_1 = \frac{\int_{-\infty}^{\infty} F_0(\tau)F_1^*(\tau)d\tau}{\int_{-\infty}^{\infty} |F_0(\tau)|^2 d\tau}. \tag{19}$$

Using Eq. (15), one easily obtains the first absorption factor for the initial Gaussian pulse

$$g_1^G(t_0,\Gamma) = \frac{\Gamma_i t_0}{\sqrt{2}} e^{\Gamma_i^2 t_0^2/2}\int_{-\infty}^{\infty} e^{-(T+\Gamma_i t_0/2)^2}[1+\mathrm{erf}(T)]dT,$$
$$= \sqrt{\frac{\pi}{2}}\Gamma_i t_0 e^{\Gamma_i^2 t_0^2/2}\mathrm{erfc}\left(\frac{\Gamma_i t_0}{\sqrt{2}}\right). \tag{20}$$

Evidently, the factor depends only on a product $\Gamma_i t_0/\sqrt{2} = \kappa$.

It turns out later that such a kind of dependence is characteristic of Gaussian absorption factors of all orders p. Using (15), we cannot express the higher-order absorption factors in the closed form. However, the required convolutions can be calculated numerically for any initial pulse shape. Later we show that by transferring the problem to the spectral domain, the closed-form expression for the g_p^G factor is obtained for any p.

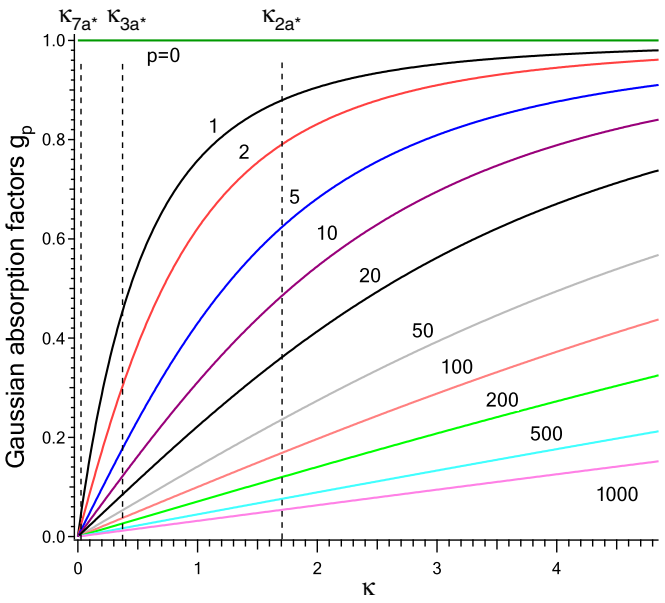

FIG. 2. Gaussian absorption factors $g_p^G(\kappa)$ for $p \leqslant 1000$. For $p \neq 1$ numerical calculation is avoided by using the analytical formula (32), which is derived later on. The dashed vertical lines denote κ values for an initial Gaussian pulse with a 100-fs FWHM intensity profile tuned to the $2a^*$ ($\kappa_{2a^*} = 1.71$), $3a^*$ ($\kappa_{3a^*} = 0.37$), and $7a^*$ ($\kappa_{7a^*} = 0.03$) states in He.

The Gaussian absorption factors $g_p^G(\kappa)$ are reported in Fig. 2 for $\kappa \leqslant 5$. One notes that for all p, $\lim_{\kappa\to\infty} g_p^G = 1$, in agreement with the corresponding limit of the closed-form expression (32). Again, when the initial pulse duration is much longer than the resonance lifetime, the dependence of the pulse intensity on the target depth becomes $I(z) = I(0)e^{-2\beta_i z/\Gamma_i}$, exactly in agreement with the BL law (3) in the $\Gamma_i \to \infty$ limit. Independent of the κ value, when $2\beta_i z/\Gamma_i \ll 1$, the first term of the expansion (17) is usually enough to describe pulse attenuation, giving approximately $I(z) \approx I(0)(1 - 2\beta_i z g_1/\Gamma_i)$. When $2\beta_i z/\Gamma_i$ is increased, higher-order terms start to contribute and the total intensity at the target exit (17) is obtained by summing their contributions

$$I(z) = I(0)\left[1 - \frac{2\beta_i z}{\Gamma_i}\frac{g_1}{1!} + \left(\frac{2\beta_i z}{\Gamma_i}\right)^2 \frac{g_2}{2!} - \left(\frac{2\beta_i z}{\Gamma_i}\right)^3 \frac{g_3}{3!} + \cdots\right]. \tag{21}$$

Note that for a given target parameter $2\beta_i z/\Gamma_i = p_0$, the absorption factors with $p \approx p_0$ contribute most importantly to Eq. (21). Figure 3 shows the dependence of the total transmitted intensity on target thickness for a Gaussian pulse tuned to three bound states featuring lifetime much shorter ($2a^*$) than, about equal ($3a^*$) to, and much longer ($7a^*$) than the initial pulse duration.

B. Spectral domain

Excited states with longer lifetimes have narrower spectral widths and the increasingly larger number of photons from the pulse just cannot be absorbed due to the energy conservation.

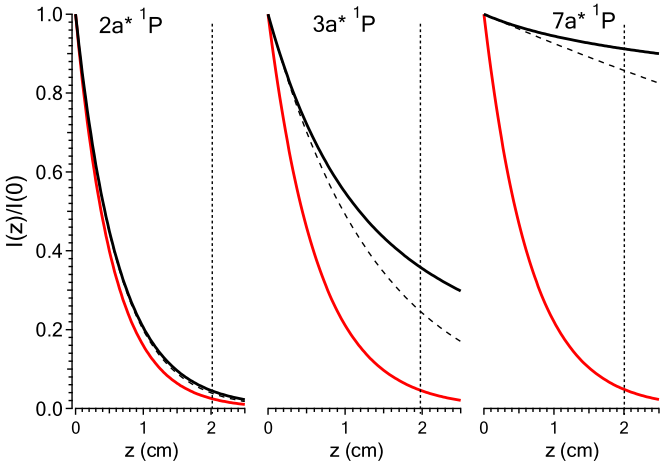

FIG. 3. Intensity attenuation for the 100-fs initial Gaussian pulse tuned to the $2a^*$, $3a^*$, and $7a^*$ resonances as a function of target thickness at a He pressure of 1000 Pa. Reported are the exponential attenuation profile $e^{-2\beta_i z/\Gamma_i}$ (red thick curve), the one-term approximation (dashed black curve), and the 100-term approximation to (17) (thick black curve). Vertical dashed lines denote a target thickness $z_0 = 2$ cm, corresponding to data presented in Fig. 1.

This simple fact explains weaker photoabsorption in the case of a narrow $7a^*$ bound state (Fig. 3). The Fourier transform allows us to attribute to each correction $F_n(\tau)$ the corresponding spectral representation $\mathcal{F}[F_n(\tau)] = S_n(\omega)$. Since the transform is linear, the spectral representation of the field amplitude is easily obtained from Eq. (10). After applying the convolution theorem, the equalities

$$\mathcal{F}[F(z,\tau)] = \mathcal{F}[F_0] - \frac{\beta_i z}{\Gamma_i}\mathcal{F}[E]\mathcal{F}[F_0] + \frac{\beta_i^2 z^2}{2\Gamma_i^2}\mathcal{F}[E]^2\mathcal{F}[F_0] + \cdots, \tag{22}$$

$$S(z,\omega) = \sum_{n=0}^{\infty}(-1)^n \frac{\beta_i^n z^n}{n!\Gamma_i^n} S_n(\omega)$$

are obtained, where $S_n(\omega) = \mathcal{F}[F_0](\mathcal{F}[E])^n \equiv S_0 s_n$. Similar to Eq. (17), the spectrum of the pulse is given by

$$|S(z,\omega)|^2 = |S_0(\omega)|^2 \sum_{p=0}^{\infty}(-1)^p \frac{\beta_i^p (2z)^p C_p(\omega)}{p!\Gamma_i^p}, \tag{23}$$

where

$$C_p(\omega) = 2^{-p}\sum_{q=0}^{p}\binom{p}{q}\mathrm{Re}[s_q(\omega)s_{p-q}^*(\omega)]. \tag{24}$$

Again, $C_0 = 1$ for all the pulse shapes and

$$s_n = \frac{(\Gamma_i/2)^n}{(\Gamma_i/2 - i\omega)^n}, \tag{25}$$

$$\mathrm{Re}[s_q(s_{p-q})^*] = \frac{\Gamma_i^p \cos[(2q-p)\arctan(2\omega/\Gamma_i)]}{(\omega^2 + \Gamma_i^2/4)^{p/2}}, \tag{26}$$

$$C_p(\omega) = \frac{(\Gamma_i/2)^{2p}}{(\omega^2 + \Gamma_i^2/4)^p}. \tag{27}$$

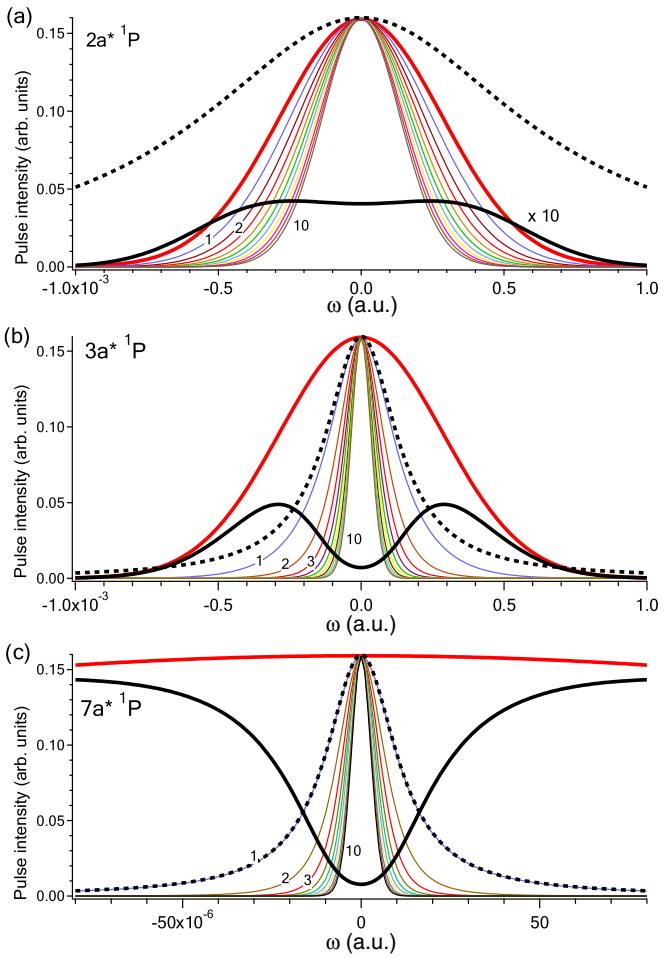

FIG. 4. Spectrum of the 100-fs Gaussian pulse tuned to the (a) $2a^*$, (b) $3a^*$, and (c) $7a^*$ resonances. The entrance spectrum [thick red (gray) curve] and the exit spectrum after passing 1 cm of He gas at 2000 Pa (thick black curve) are given. Thin curves denote the lowest ten spectral base intensity functions $|S_0(\omega)|^2 C_p(\omega)$. They are normalized to the same amplitude and denoted by order $1 \leqslant p \leqslant 10$. In this specific example the converged final spectrum is built up from 25 base functions, weighted according to Eq. (23). The black dotted curve denotes the Lorentzian profile of the corresponding resonance.

In analogy with the time domain [Eq. (18)], the pth spectral base intensity function $|S_0(\omega)|^2 C_p(\omega)$ is given by the product of the initial spectral intensity and a Lorentzian to the pth power. This is completely in agreement with the BL law for a single bound state, as can be seen by expanding the exponential factor in Eq. (2). In Fig. 4 the spectral base intensity functions are presented for the three bound states in He, as well as the pulse spectrum after traveling through the same target thickness as presented in Fig. 1. In general, the higher p is, the narrower and smaller the corresponding spectral base function is, resembling more a Gaussian. When $2\beta_i z/\Gamma_i \ll 1$, the spectral base intensity function with $p = 1$ most importantly modifies the initial profile, so

$$|S(z,\omega)|^2 \approx |S_0(\omega)|^2 \left(1 - \frac{2\beta_i z C_1(\omega)}{\Gamma_i}\right). \tag{28}$$

For an initial Gaussian pulse $|S_0^G(\omega)|^2 = (2\pi)^{-1} e^{-2t_0^2\omega^2}$, the modified profile is given by

$$|S(z,\omega)|^2 \approx \frac{e^{-2t_0^2\omega^2}}{2\pi}\left(1 - \frac{\beta_i \Gamma_i z}{2\left(\omega^2 + \Gamma_i^2/4\right)}\right). \tag{29}$$

There is an important difference between the temporal and spectral descriptions of the problem. While the initial pulse shape is encoded in each temporal base field function $F_n(\tau)$ by means of multiple convolutions with the exponential decay function, in the spectral domain, the initial pulse profile is present only as a multiplicative factor in every base function. Consequently, the attenuated spectral profile is a product of the initial pulse profile and exponential factor $\exp[-2\beta_i C_1(\omega) z/\Gamma_i]$, resulting in the BL law (2). Contrary to the frequency component of the pulse, attenuation of a given temporal component is related not only to its initial intensity, but also to the pulse intensity at previous times, via a buildup of exponentially decaying atomic coherence. The BL law in the time domain may then be written as

$$I(z,\tau) = |F_0(\tau)|^2 - (1 - e^{-\sigma_i(\omega_i) N z \hat{G}}) F_0(\tau), \tag{30}$$

where $\hat{G}^p F_0(\tau) \equiv G_p(\tau)$. Note that the set of temporal base intensity functions $G_p(\tau)$ [Eq. (18)] is different for different initial pulse profiles $F_0(\tau)$, which makes the application of Eq. (30) less practical than its spectral version [Eq. (2)].

The integral of spectral intensity is proportional to the total photon intensity, so

$$\int_{-\infty}^{\infty} |S(z,\omega)|^2 d\omega = \int_{-\infty}^{\infty} |F(z,\tau)|^2 d\tau$$

must hold for each z. In other words, the spectral representation must result in exactly the same target depth intensity dependence as given by the representation in the time domain [Eq. (21)]. Consequently, for a Gaussian case, the following equality must hold for each p:

$$\frac{(\Gamma_i/2)^{2p}}{2\pi} \int_{-\infty}^{\infty} \frac{e^{-2t_0^2\omega^2}}{\left(\omega^2 + \Gamma_i^2/4\right)^p} d\omega = \frac{g_p^G(t_0, \Gamma_i)}{2t_0\sqrt{2\pi}}. \tag{31}$$

Indeed, by inserting (20) and integrating, Eq. (31) is seen to hold exactly for $p = 1$. For low values of p, the validity of (31) was checked numerically. Since the integral on the left-hand side can be given in the closed form (see Ref. [16], Sec. 3.383/4), one may use the above equality to calculate Gaussian absorption factors

$$g_p^G(\kappa) = \kappa^{p-1/2} e^{\kappa^2/2} W_{1/4-p/2,1/4-p/2}(\kappa^2). \tag{32}$$

Above, $W_{\alpha,\beta}(z)$ is the Whittaker function (see [17], p. 505). For $p = 1$ the function is related to the error function through

$$W_{-1/4,-1/4}(x > 0) = e^{x/2} \mathrm{erfc}(\sqrt{x}) \sqrt{\pi\sqrt{x}}. \tag{33}$$

The Whittaker functions for $p \geqslant 2$ are calculated recursively using

$$W_{\lambda-1/2,\lambda-1/2}(x) = \frac{[\lambda - (1-x)/2] W_{\lambda,\lambda}(x) + x W'_{\lambda,\lambda}(x)}{2\sqrt{x}(\lambda - 1/4)}, \tag{34}$$

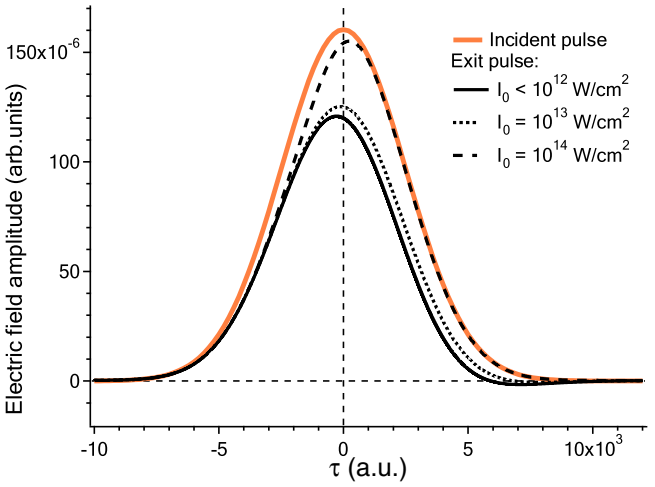

FIG. 5. Dependence of electric field amplitude on I_0, the initial pulse intensity, after passing 1 cm of He gas at 400 Pa (black curves). The initial Gaussian pulse (red curve) is resonant with the $0 \rightarrow 2a^*$ transition.

starting with (33) and its derivative

$$W'_{-1/4,-1/4}(x) = -\frac{e^{-x/2}}{x^{1/4}} + \sqrt{\pi} e^{x/2}\left(\frac{1}{4x^{3/2}} + \frac{x^{1/4}}{2}\right)\mathrm{erfc}(\sqrt{x}). \quad (35)$$

The lowest Gaussian absorption factors are seen to be

$$g_1^G(\kappa) = \kappa\sqrt{\pi} e^{\kappa^2}\mathrm{erfc}(\kappa),$$

$$g_2^G(\kappa) = \kappa^2 - \sqrt{\pi} e^{\kappa^2}\left(\kappa^3 - \frac{\kappa}{2}\right)\mathrm{erfc}(\kappa),$$

$$g_3^G(\kappa) = -\frac{\kappa^4}{2} + \frac{3\kappa^2}{4} + \sqrt{\pi} e^{\kappa^2}\left(\frac{\kappa^5}{2} - \frac{\kappa^3}{2} + \frac{3\kappa}{8}\right)\mathrm{erfc}(\kappa),$$

$$g_4^G(\kappa) = \frac{\kappa^6}{6} - \frac{\kappa^4}{3} + \frac{5\kappa^2}{8} - \sqrt{\pi} e^{\kappa^2}\left(\frac{\kappa^7}{6} - \frac{\kappa^5}{4} + \frac{3\kappa^3}{8} - \frac{5\kappa}{16}\right)\mathrm{erfc}(\kappa).$$

The spectral and temporal profiles of the attenuated pulse relative to the incident pulse do not depend on the initial light intensity, as long as the weak-light assumption holds. We have calculated the temporal profile of the attenuated pulse by solving numerically the complete set of MB equations for the two-level system (see [7]), taking into account nonlinear processes such as stimulated emission, as appropriate for high incident light intensity. The result in Fig. 5 shows that under the chosen conditions, a light intensity as high as 10^{12} W/cm^2 may be considered weak.

C. Input pulse with an arbitrary phase distribution

To check the validity of Eq. (10) numerically for weak-light pulses with arbitrary distribution of phases, we have generated eight different sets of pulses by a partial-coherence method [19]. The method was shown to generate short pulses corresponding to those at the output of the real free-electron-laser (FEL) facility with the self-amplified spontaneous emission source. Briefly, pulse generation for a given set starts by assigning the pulse field in the spectral space: The amplitude was selected according to the Gaussian of a given width and the phase was randomly selected. The field was then converted to the time domain by means of a Fourier transform. Finally, the field amplitude was filtered by a Gaussian with the width corresponding to duration of the FEL pulse.

On average, each of the sets gives a smooth Gaussian spectrum and all the sets on average display the same 100-fs broad Gaussian temporal intensity profile. Figure 6(a) presents an absolute square of the normalized autocorrelation function (4),

$$\gamma_n(\Delta) = \frac{\gamma(\Delta)}{\int_{-\infty}^{\infty} dt\sqrt{|F(t)F(t+\Delta)|^2}}, \quad (36)$$

averaged over 300 pulses for each set. The sets are ordered from the least coherent one, denoted by set 1, to the fully coherent set 8. Although all the pulse sets have the same average temporal intensity profile (marked by 0), one can see in Fig. 6(b) that an average attenuation level and the outgoing temporal profile are sensitive to the degree of coherence of the initial pulse. For fully coherent pulses, the strongest delayed contribution due to the FID is observed in the tail of the pulse. Note that the result for set 8 corresponds to the result in Fig. 1(b), upon squaring the field amplitude. For an almost incoherent set of pulses, the FID contribution practically disappears because the coherence ρ_{0i} cannot build up in the presence of an electric field with a randomly varying phase. The observation of the attenuated temporal profile therefore allows us to estimate the degree of temporal coherence of the initial pulse.

Finally, one of the generated initial pulses, a member of pulse set 3, was propagated by means of Eq. (10) to reconstruct its temporal intensity profile at the target exit. According to Eq. (18), the base intensity profiles G_p, corresponding to the selected initial pulse, were constructed first [Fig. 7(a)]. In contrast to the previously studied case presented in Fig. 1, a more general situation considered here leads to the sign-changing base pulses for small values of the expansion index p. The temporal base intensity profiles were inserted in the nonintegrated version of Eq. (17) [see also Eq. (48) below] to obtain the temporal dependence of the corresponding exit pulse for the chosen target conditions. As shown in Fig. 7(b), a substantial redistribution of the pulse intensity in time occurs upon passing the target: Although the total intensity at the target exit is smaller than the total initial intensity, the exit intensity at particular times τ may be higher than the initial intensity. Note that pulse intensity at the target exit is positive at all times only when the number of terms included in the expansion (49) is large enough. The convergence to the final pulse profile is the slowest at large times τ where weak higher-order contributions dominate [Fig. 7(a)].

III. FANO RESONANCE

The previous examples deal with bound states exhibiting excitation energies and decay widths of $^1P_1$ doubly excited states $2a$, $3a$, and $7a$ below the $N = 2$ ionization threshold in He. However, these strongly autoionizing states are in fact Fano resonances displaying an asymmetric photoabsorption cross

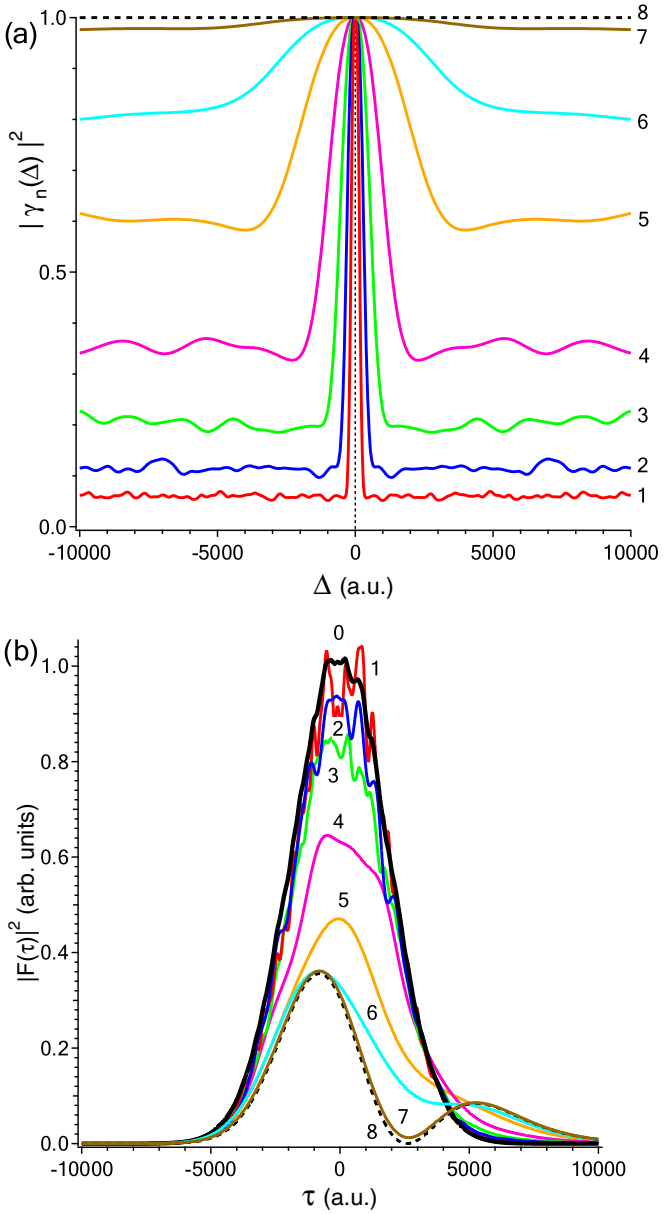

FIG. 6. (a) Absolute square of the autocorrelation function for a variety of input light pulses marked from 1 (almost incoherent) to 8 (fully time coherent). In all the cases the initial intensity profile of the pulse is a Gaussian with a 100-fs FWHM. (b) Comparison of intensity profiles of the initial (0) and the outgoing pulses (1–8) after passing a 2-cm-long target. The target is filled with 1000 Pa of He and the average initial pulse is tuned to the $3a^*$ resonance. For each set, the presented outgoing profile is an average of 300 pulses. The incident profile is an average of all 2400 pulses.

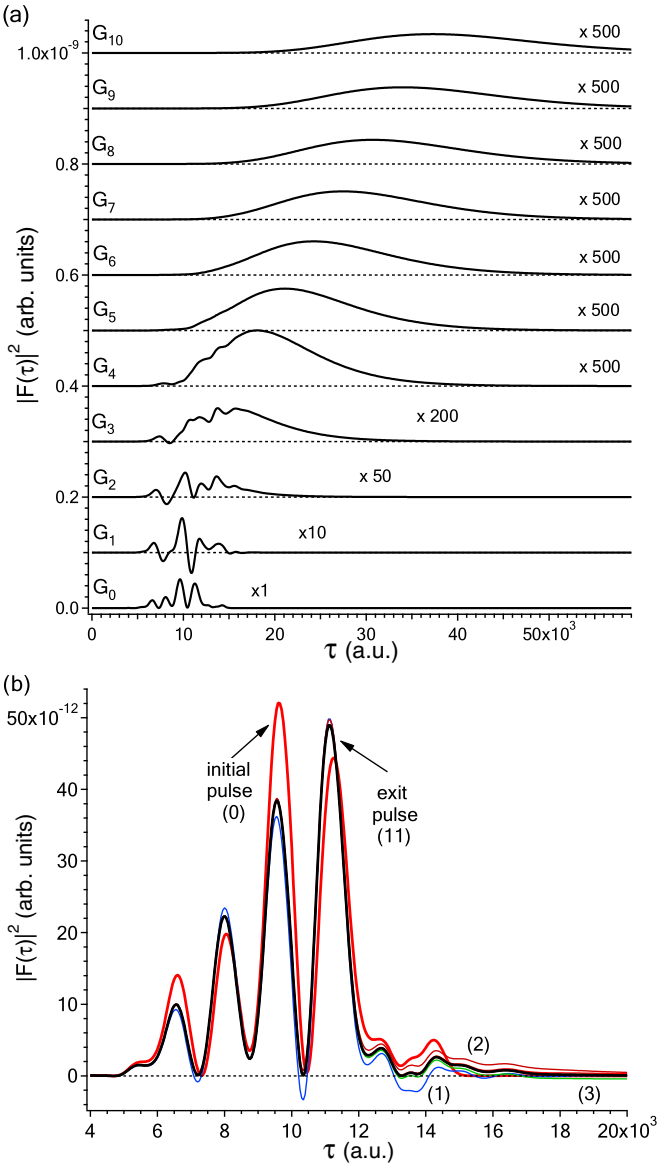

FIG. 7. (a) Lowest 11 temporal base intensity functions $G(\tau)$ of a single partially coherent entrance pulse G_0, randomly selected from the set 3 in Fig. 6. (b) "Evolution" of the pulse profile from its initial form to the exit form by adding up the temporal base intensity functions, each weighted by $(-2\beta_i z)^p/p!\Gamma_i^p$. Under the same target conditions as in Fig. 6, the sum of (p) terms converges to the numerically propagated exit pulse (thick black line) after summing up to $p = 10$.

section $\sigma^f = \sigma_c(q_i+\epsilon)^2/(\epsilon^2+1)$ rather than a Lorentzian [14]. The Fano parameter q_i determines asymmetry of the profile, $\epsilon = 2(\omega-\omega_i)/\Gamma_i$ is the reduced energy, and $\sigma_c = 4\pi^2\alpha\omega_i|d_{0c}|^2$ represents a smooth continuum photoabsorption cross section close to the resonance energy ω_i, which is perturbed by an admixture of a discrete state. Knowing the photoabsorption profile, one can immediately write down the spectral profile of the attenuated pulse by using the BL law (2),

$$I(z,\omega) = I_{\omega_i}(0,\omega)\sum_{n=0}^{\infty}\frac{\left[-\sigma_c N z\left(\omega-\omega_i+\frac{\Gamma_i q_i}{2}\right)^2\right]^n}{n!\left[(\omega-\omega_i)^2+\frac{\Gamma_i^2}{4}\right]^n}, \quad (37)$$

as well as the total pulse intensity at the target exit (3),

$$I(z) = \sum_{n=0}^{\infty}\frac{(-\sigma_c N z)^n}{n!}\int_0^{\infty}d\omega\frac{I_{\omega_i}(\omega,0)\left(\omega-\omega_i+\frac{\Gamma_i q_i}{2}\right)^{2n}}{\left[(\omega-\omega_i)^2+\frac{\Gamma_i^2}{4}\right]^n}. \quad (38)$$

The exit spectrum of the pulse tuned to the $3a\ ^1P_1$ resonance in Fig. 8(a) can be readily understood. A comparison with the

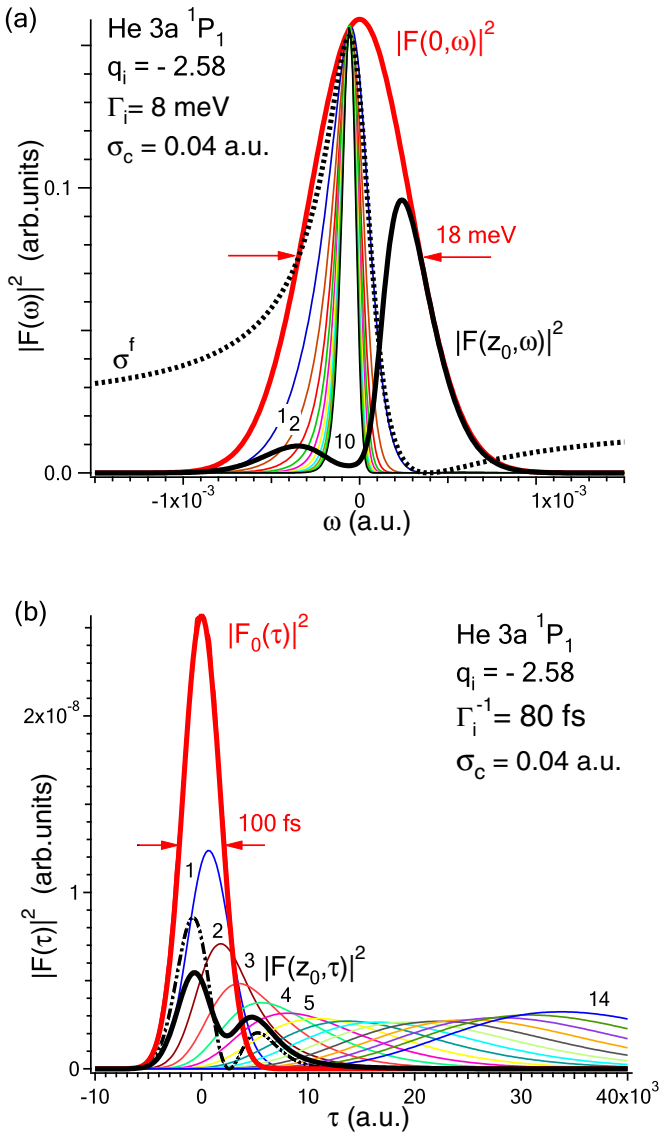

FIG. 8. Intensity of the 100-fs Gaussian pulse tuned to the $3a\ ^1P_1$ resonance in He after passing $z_0 = 2$ cm of gas at 1000 Pa. The pulse at the entrance (red thick curve) is compared to the exit pulse (black thick curve) in (a) the spectral domain, where thin (multicolored) lines denote spectral base intensity functions for the selected initial pulse, extracted from (37) and denoted by the summation index n, and (b) the time domain, where thin (multicolored) lines denote temporal base intensity functions $\tilde{G}_p(\tau)$ (50) for $1 \leqslant p \leqslant 14$, needed to obtain the convergent exit pulse. The dash-dotted line is the exit pulse profile due to absorption by an "equivalent" pure bound-state resonance $3a^*$.

result for the (assumed) Lorentzian profile (the middle graph in Fig. 4) shows that the maximum absorption point has shifted by $\Gamma_i/2q_i$. The pulse profile is asymmetric with no attenuation at $\omega - \omega_i = -\Gamma_i q_i/2$, where the Fano profile falls to zero.

Next we construct the intensity profile of the attenuated pulse tuned to the Fano resonance in the time domain. The field equation (6) is cast in the form

$$\frac{1}{c}\frac{\partial F}{\partial t} + \frac{\partial F}{\partial z} = \frac{2\pi i \omega_i}{c}\int_{-\infty}^{\infty} \chi(t')F(z,t-t')dt', \tag{39}$$

where the linear susceptibility $\chi(t)$ depends only on properties of the atomic medium (see Ref. [7], p. 181). For a resonant transition to a single bound state (9), the susceptibility is therefore given by an exponential decay function

$$\chi(t) = iN\rho_{00}|d_{0i}|^2 e^{-\Gamma_i t/2}\Theta(t), \tag{40}$$

where $\Theta(t)$ denotes the Heaviside step function. The Fourier transform $\mathcal{F}[\chi(t)]$ of (40) gives the corresponding spectral form

$$\chi(\omega) \propto -\frac{(\omega-\omega_i)\frac{\Gamma_i}{2}}{(\omega-\omega_i)^2+\frac{\Gamma_i^2}{4}} + i\frac{\frac{\Gamma_i^2}{4}}{(\omega-\omega_i)^2+\frac{\Gamma_i^2}{4}}. \tag{41}$$

The real and imaginary parts of (41) describe field dispersion and absorption, respectively, the latter giving the well-known Lorentzian line profile.

The time-dependent susceptibility for an isolated Fano resonance is calculated starting from the imaginary part of the corresponding spectral form, the Fano absorption profile σ^f. Following the treatment of Ref. [20], the real part of spectral susceptibility is generated by the Kramers-Kronig relation to recover its full (complex) form

$$\begin{aligned}\chi^f(\omega) \propto{}& \frac{(\omega-\omega_i)\left(1-q_i^2\right)\frac{\Gamma_i}{2}+\frac{q_i\Gamma_i^2}{2}}{(\omega-\omega_i)^2+\frac{\Gamma_i^2}{4}} \\ &+ i\frac{\left(q_i^2-1\right)\frac{\Gamma_i^2}{4}+(\omega-\omega_i)q_i\Gamma_i}{(\omega-\omega_i)^2+\frac{\Gamma_i^2}{4}} \\ &+ \lim_{\mu\to\infty}\left(-\frac{(\omega-\omega_i)\frac{\mu}{2}}{(\omega-\omega_i)^2+\frac{\mu^2}{4}} + i\frac{\frac{\mu^2}{4}}{(\omega-\omega_i)^2+\frac{\mu^2}{4}}\right).\end{aligned} \tag{42}$$

Note that the contribution of the nonresonant continuum σ_c to the Fano cross section σ^f was formally replaced by the contribution of a broad discrete state ($\mu \to \infty$), which results in terms of the same form as in Eq. (41). The Fourier transform of Eq. (42) leads to

$$\chi^f(t) \propto i\left((q_i-i)^2\frac{\Gamma_i}{2}e^{-\Gamma_i t/2} + \lim_{\mu\to\infty}\left[\frac{\mu}{2}e^{-\mu t/2}\right]\right)\Theta(t). \tag{43}$$

Taking the limit and comparing the result to Eqs. (39) and (40), the temporal response of the Fano resonance in the weak-field regime is given by

$$\chi^f(t) = \frac{iN|\tilde{d}_{0i}|^2}{q_i^2}\left((q_i-i)^2 e^{-\Gamma_i t/2} + \frac{2}{\Gamma_i}\delta(t)\right)\Theta(t). \tag{44}$$

The continuum dipole matrix element in σ_c was expressed with the dipole matrix element $\tilde{d}_{0i}$ between the ground and the modified discrete state using the relation $|d_{0c}|^2 = 2|\tilde{d}_{0i}|^2/\pi q_i^2\Gamma$ [14]. The resonant field impulse excitation therefore triggers a twofold temporal response of an isolated Fano state: a prompt one and an exponentially decaying one, the latter being determined by the autoionization decay width Γ_i. For a Fano resonance, the analog of Eq. (9) is therefore

$$\begin{aligned}\frac{\partial F}{\partial z} = -\frac{\tilde{\beta}_i}{2}\int_{-\infty}^{\tau} F(z,\tau') \\ \times\left[\frac{2\delta(\tau-\tau')}{\Gamma_i q_i^2} + \left(1-\frac{i}{q_i}\right)^2 e^{-\Gamma_i(\tau-\tau')/2}\right]d\tau',\end{aligned} \tag{45}$$

where $\tilde{\beta}_i = 4\pi\omega_i|\tilde{d}_{0i}|^2 N = \sigma_c N\Gamma_i q_i^2/2$. Equation (45) reduces properly in both limiting cases: When $q_i \to \infty$, the result coincides with the result (9) for a pure bound state because $|\tilde{d}_{0i}|^2 = |d_{0i}|^2 q_i^2/(q_i^2-1)$ [14]; in the limit $q_i \to 0$, Eq. (45) becomes

$$\frac{\partial F}{\partial z} = \frac{-\sigma_c N}{2}\left(F(z,\tau) - \frac{\Gamma_i}{2}\int_{-\infty}^{\tau} e^{-\Gamma_i(\tau-\tau')/2}F(z,\tau')d\tau'\right). \tag{46}$$

This is the expected behavior of the "window resonance" in the spectral domain, composed of a flat continuum where the absorption is locally annihilated by an upside-down Lorentzian profile. Indeed, when the profile is very broad ($\Gamma_i \to \infty$), the integral on the right-hand side of Eq. (46) evaluates to $F(z,\tau)$ and the absorption reduces to zero.

Similar to Eq. (10), the solution of Eq. (45) is given by

$$\begin{aligned} F(z,\tau) &= F_0(\tau) - \frac{\tilde{\beta}_i z}{\Gamma_i}[\tilde{E} * F_0](\tau) + \frac{\tilde{\beta}_i^2 z^2}{2\Gamma_i^2} \\ &\quad \times [\tilde{E} * \tilde{E} * F_0](\tau) + \cdots \\ &= \sum_{n=0}^{\infty}(-1)^n \frac{\tilde{\beta}_i^n z^n}{n!\Gamma_i^n}\tilde{F}_n(\tau), \end{aligned} \tag{47}$$

where $\tilde{F}_n$ denotes the convolution of the n-fold convolution of

$$\tilde{E}(\tau) = \frac{\delta(\tau)}{q_i^2} + \left(1 - \frac{i}{q_i}\right)^2 \frac{\Gamma_i}{2} e^{-\Gamma_i\tau/2}$$

with the initial pulse $F_0(\tau)$. In fact, by inspecting the form of the solution (8), one can express $\tilde{F}_n$ as a linear combination of convolutions F_n [see Eq. (12)], describing the solution for a pure bound state

$$\tilde{F}_n(\tau) = q_i^{-2n}\sum_{n'=0}^{n}\binom{n}{n'}(q_i - i)^{2n'}F_{n'}(\tau). \tag{48}$$

We proceed by calculating the temporal profile of the field intensity

$$|F(z,\tau)|^2 = \sum_{p=0}^{\infty}\frac{(-2\tilde{\beta}_i z)^p}{\Gamma_i^p\, p!}\tilde{G}_p(\tau) \tag{49}$$

in the same way as before, inserting $\tilde{F}_n$ instead of F_n into Eq. (18). Using Eq. (48), the temporal base intensity functions $\tilde{G}_p$ for a Fano resonance can be expressed by a linear combination of temporal base field functions (12) for a Lorentzian:

$$\begin{aligned} \tilde{G}_p(\tau) &= 2^{-p}\sum_{p'=0}^{p}\binom{p}{p'}\tilde{F}_{p'}(\tau)\tilde{F}^*_{p-p'}(\tau) \\ &= q^{-2p}\sum_{r=0}^{[p/2]}\sum_{r'\geqslant r}^{p-r}\left[2^{-(r+r')}(2-\delta_{rr'})\binom{p}{r}\binom{p-r}{r'}\right. \\ &\quad \left.\times \mathrm{Re}[(q-i)^{2r}(q+i)^{2r'}F_r(\tau)F^*_{r'}(\tau)]\right]. \end{aligned} \tag{50}$$

Upper summation limit of the outer summation in Eq. (50) equals the greatest integer less than or equal to $p/2$. We note that in order to compose $\tilde{G}_p$, one needs to precalculate $F_n(\tau)$ for $0 \leqslant n \leqslant p$, which is needed anyway to take into account the terms up to p in the expansion.

In Fig. 8(b), the temporal intensity profile of the pulse is presented at a target depth z_0, assuming now that the state is an autoionizing resonance and the initial pulse has a Gaussian shape. This is to be compared to case 8 in Fig. 6(b), showing the exit pulse profile for the same initial pulse, resonantly tuned to a bound state. Besides the coherence properties of the initial pulse, the attenuated temporal profile obviously depends also on the nature of the excited state. Namely, for the Fano resonance featuring the same d_{0i} and Γ_i as the bound state, the delayed secondary maximum is less pronounced.

Finally, we note that the same result as (45) is obtained by replacing in MB equations (6) and (7) the dipole matrix element d_{0i} by $\tilde{d}_{0i}(1 - i/q_i)$ and adding an extra term $-\sigma_c N F/2$ to the left-hand side of Eq. (6). These modifications are consistent with the previous time-dependent studies dealing with autoionizing states [21–27].

IV. CONCLUSION

In this paper, an analog of the well-known Beer-Lambert law was discussed in the time domain. It was shown that the temporal profile of the attenuated light pulse can be obtained by weighted summation of multiple convolutions of the temporal profile of the incident pulse with the atomic response function. Instead of numerically solving the two-level system of partial differential equations describing propagation of weak light in an atomic medium, the temporal dependence of the pulse intensity at a given target depth is constructed by summing up the characteristic base functions, each weighted by the corresponding factor in the expansion of the exponential function. Assuming weak light, the method is applicable for an arbitrary atomic response and is presented here for the incident light pulses in resonance with a single bound-bound and bound-Fano state transition, respectively. The case with the coherent 100-fs incident Gaussian pulse was treated in detail and illustrated by transitions from the ground to the selected doubly excited states in the He atom featuring different lifetimes with respect to the incident pulse duration. A general applicability of the method was demonstrated by working out the attenuation of an arbitrary incident pulse using both a direct numerical integration of differential equations and construction of the pulse profile from the corresponding set of temporal base intensity functions. The latter approach offers additional insight into the pulse transformation process: By increasing the target thickness, the higher-order base functions in the expansion are gradually "switched on," causing characteristic modifications of the pulse profile. The relation and the complementarity of the method to the spectral domain approach was briefly discussed. Current applications may include analysis of captured intensity profiles of attenuated pulses with initial duration in the nanosecond to picosecond range, possibly reaching the femtosecond timescale with future development of instrumentation. The method may also be useful in the analysis of pump-probe experiments where it is important to follow changes in the initial pulse temporal profile with the target depth.

ACKNOWLEDGMENTS

This work was supported by P1-0112 Research Program and J1-8134 Research Project of the Slovenian Research Agency (ARRS).

[1] D. N. Sathyanarayana, *Electronic Absorption Spectroscopy and Related Techniques* (Universities Press, Hyderabad, 2001).
[2] P. Bouguer, *Essai d'Optique sur la Gradation de la Lumire* (Jombert, Paris, 1729), pp. 16–22.
[3] J. H. Lambert, *Photometria Sive de Mensura et Gradibus Luminis, Colorum et Umbrae (Photometry, or, On the Measure and Gradations of Light, Colors, and Shade)* (Klett, Augsburg, 1760).
[4] A. Beer, Ann. Phys. Chem. **86**, 78 (1852).
[5] A. F. Starace, in *Theory of Photoionization*, edited by W. M. S. Flügge, Handbuch der Physik Vol. XXI (Springer, Berlin, 1982).
[6] J. M. Hollas, *Modern Spectroscopy*, 4th ed. (Wiley, New York, 2004).
[7] P. Lambropoulos and D. Petrosyan, *Fundamentals of Quantum Optics and Quantum Information* (Springer, Berlin, 2007).
[8] D. C. Champeney, *Power Spectra and Wiener's Theorems: A Handbook of Fourier Theorems* (Cambridge University Press, Cambridge, 1987).
[9] J. Kauppinen and D. Partanen, *Fourier Transforms in Spectroscopy* (Wiley-VCH Verlag GmbH, Wienheim, 2001).
[10] J. S. Courtney-Pratt, Research **2**, 287 (1949).
[11] O. Zandi, K. J. Wilkin, and M. Centurion, Rev. Sci. Instrum. **88**, 063305 (2017).
[12] R. G. Brewer and R. L. Shoemaker, Phys. Rev. A **6**, 2001 (1972).
[13] S. Bengtsson, E. W. Larsen, D. Kroon, S. Camp, M. Miranda, C. L. Arnold, A. L'Huillier, K. J. Schafer, M. B. Gaarde, L. Rippe, and J. Mauritsson, Nat. Photon. **11**, 252 (2017).
[14] U. Fano, Phys. Rev. **124**, 1866 (1961).
[15] A. K. Hussain, F. S. Fadhel, Z. R. Yahya, and N. Rusli, J. Theor. Appl. Inf. Technol. **88**, 367 (2016).
[16] I. S. Gradshteyn and I. M. Ryzhik, *Table of Integrals, Series and Products* (Academic Press, New York, 1994).
[17] J. L. Slater, in *Handbook of Mathematical Functions With Formulas, Graphs and Mathematical Tables*, 10th ed., Natl. Bur. Stand. (US) Appl. Math. Ser. 55, edited by M. Abramowitz and I. A. Stegun (US GPO, Washington, DC, 1972), Chap. 13, p. 503.
[18] A. Mihelič, Ph.D. thesis, University of Ljubljana, 2006, available at http://www.rcp.ijs.si/amihelic/phd/thesis.pdf.
[19] T. Pfeifer, Y. Jiang, S. Dusterer, R. Moshammer, and J. Ullrich, Opt. Lett. **35**, 3441 (2010).
[20] C. Ott, A. Kaldun, P. Raith, K. Meyer, M. Laux, J. Evers, C. H. Keitel, C. H. Greene, and T. Pfeifer, Science **340**, 716 (2013).
[21] P. Lambropoulos and P. Zoller, Phys. Rev. A **24**, 379 (1981).
[22] G. Alber and P. Zoller, Phys. Rev. A **27**, 1373 (1983).
[23] G. S. Agarwal, S. L. Haan, and J. Cooper, Phys. Rev. A **29**, 2552 (1984).
[24] T. Nakajima and P. Lambropoulos, Phys. Rev. A **50**, 595 (1994).
[25] E. Paspalakis, N. J. Kylstra, and P. L. Knight, Phys. Rev. A **60**, 642 (1999).
[26] T. Nakajima and G. Buica, Phys. Rev. A **71**, 013413 (2005).
[27] A. Mihelič, M. Žitnik, and M. Hrast, J. Phys. B **50**, 245602 (2017).